Journal of Non-Crystalline Solids 525 (2019) 119575

Contents lists available at ScienceDirect

Journal of Non-Crystalline Solids

journal homepage: www.elsevier.com/locate/jnoncrysol

Time-dependent nucleation rate measurements in $BaO{\cdot}2SiO_2$ and $5BaO{\cdot}8SiO_2$ glasses

Xinsheng Xia[a,*], D.C. Van Hoesen[b], Matthew E. McKenzie[c], Randall E. Youngman[c], Ozgur Gulbiten[c], K.F. Kelton[a,b]

[a] Institute of Materials Science and Engineering, Washington University, St. Louis, MO 63130, USA
[b] Department of Physics, Washington University, St. Louis, MO 63130, USA
[c] Science and Technology Division, Corning Incorporated, Corning, NY 14831, USA

ARTICLE INFO

Keywords:
Nucleation rate measurement
Barium silicate glasses
Critical work of cluster formation

ABSTRACT

The two-step heat treatment method is used to measure the steady state crystal nucleation rate and induction time as a function of temperature in $BaO{\cdot}2SiO_2$ and $5BaO{\cdot}8SiO_2$ glasses. For both glasses, the temperature for maximum nucleation rate and the temperature range for significant nucleation agree well with previous estimates from differential thermal analysis studies. The data are analyzed with a new iterative method to obtain the interfacial free energy and critical work of cluster formation as a function of temperature. For temperatures below the temperature at which steady-state nucleation rate is a maximum, the critical work of cluster formation is shown to strongly deviate from expectations of the classical theory of nucleation.

1. Introduction

Understanding and controlling crystal nucleation is critically important for the manufacturing of glass and glass-ceramic products [1–3]. Nucleation and growth of crystal phases must be effectively suppressed for glass formation and subsequent processing, as well as to ensure long-term stability of the glass products. For glass-ceramics, nucleation and growth must be precisely controlled to produce the desired devitrified microstructures, including the number, type, and size of crystallites formed in the glass-ceramics [4–7]. Currently, the knowledge of how to control nucleation is largely gained from empirical studies. Improved models beyond the commonly used Classical Theory of Nucleation (CNT), which is known to be significantly flawed [8], are needed. The development of these more advanced models, however, is partially hindered by the lack of experimental data over a wide range of silicate glasses.

In this publication, we present new time-dependent nucleation data in two barium silicate glasses. The data were obtained using a two-step heat-treatment method [9,10], in which glasses are first heated isothermally at a temperature that is near the peak nucleation rate (the nucleation step). The nuclei formed there do not grow significantly since the growth rates are very small at this temperature. To grow them to observable size, the nucleated glasses are given a heat treatment at a second, higher, temperature where the growth rate is large, but the nucleation rate is small (the growth step).

While the nucleation rate has been measured in $BaO{\cdot}2SiO_2$ glasses in several previous studies [11–13], those results suffer from a lack of sufficient data to accurately obtain the steady state nucleation rate and one case reports inconsistent results. Further, no measurements of the nucleation rate in $5BaO{\cdot}8SiO_2$ glasses exist. In this work, the steady state nucleation rate and the induction time are measured as a function of temperature in $BaO{\cdot}2SiO_2$ and $5BaO{\cdot}8SiO_2$ glasses. The results are in agreement with previous estimates of the temperature ranges for significant nucleation and the peak temperatures in the steady-state rates obtained from differential thermal analysis (DTA) studies [14], further validating the DTA method to make quick surveys of nucleation temperatures. The experimental data are analyzed using a new iterative method to obtain the interfacial free energy and the critical work of cluster formation (nucleation barrier) as a function of temperature. As found in other silicate glasses, the interfacial free energy has a positive temperature dependence at temperatures above that of the peak nucleation rate. Below the peak nucleation temperature, the rates are different than predicted from CNT. The departure is more pronounced in these glasses than in other glasses that have been studied. They suggest that rather than continuing to decrease with decreasing temperature, the nucleation barrier first enters a plateau and then begins to rise slowly below the peak nucleation rate temperature.

* Corresponding author.
E-mail address: x.xia@wustl.edu (X. Xia).

https://doi.org/10.1016/j.jnoncrysol.2019.119575
Received 12 May 2019; Received in revised form 28 June 2019; Accepted 15 July 2019

2. Experiments

The $BaO{\cdot}2SiO_2$ and $5BaO{\cdot}8SiO_2$ glasses studied were prepared by Corning Incorporated. To produce the glasses, 2500 g batches of barium carbonate and high-purity silica were mixed in specific ratios, corresponding to the composition of each glass, and melted in platinum crucibles at 1600 °C for 6 h. These liquids were then quenched to form glasses that were broken into glass cullet. To make homogenous glasses, these were re-melted at 1500 to 1600 °C for 6 h, and then roller quenched or made into patties by pouring onto a stainless steel table. Glasses were analyzed using Inductively Coupled Plasma – Optical Emission Spectroscopy (ICP-OES) to determine the actual compositions, confirming that the $BaO{\cdot}2SiO_2$ and $5BaO{\cdot}8SiO_2$ glasses contained 33.2 and 38.8 mol% BaO, respectively. The glass transition temperature (T_g) was determined by differential scanning calorimetry (DSC) with a heating rate of 10 °C/min after cooling the samples at 10 °C/min from the supercooled liquid to room temperature. The T_g values for the two glasses are 695 °C for $BaO{\cdot}2SiO_2$ and 697 °C for $5BaO{\cdot}8SiO_2$.

One 5BaO·8SiO2 glass was heat treated at 725 °C for 97 min and then heat treated at 846 °C for 47 min to crystallize the sample. The crystallized sample surface was polished using 400 grit SiC paper, washed in water and ultrasonically cleaned in acetone. Using this sample, the enthalpy of fusion (212.3 kJ/mol) and the liquidus temperature (1446 °C) were obtained from DSC measurements using a NETZSCH DSC 404 F1 Pegasus. The temperature and heat flow sensitivity of the DSC were calibrated by using the melting point of standard metals and the phase transition points of inorganic compounds. The heat flow accuracy was further verified by using a sapphire standard. The DSC measurements were made in platinum crucibles under an inert argon atmosphere at a 10 °C/min heating rate from room temperature.

The $BaO{\cdot}2SiO_2$ and $5BaO{\cdot}8SiO_2$ glasses were cut into smaller samples for the nucleation studies. The $BaO{\cdot}2SiO_2$ samples were approximately 5 mm × 5 mm in area dimension and 1.24 ± 0.08 mm thick; the $5BaO{\cdot}8SiO_2$ had the same area dimensions and were 1.33 ± 0.15 mm thick. For the two-step heat treatments, the samples were contained in a Coors high alumina combustion boat and placed in the center zone of a Lindberg Blue M three-zone furnace. The nucleation treatments for the $BaO{\cdot}2SiO_2$ glass samples were made at 650, 675, 700, 712, 725, 738, 750 and 775 °C, for different times. The $5BaO{\cdot}8SiO_2$ glass samples were nucleated at 675, 700, 712, 725, 738, 750 and 775 °C, also for different times. After the nucleation treatment, the $BaO{\cdot}2SiO_2$ and $5BaO{\cdot}8SiO_2$ samples and the container were taken out from the furnace and cooled to room temperature on a metal plate in air under ambient pressure. Then the $BaO{\cdot}2SiO_2$ and $5BaO{\cdot}8SiO_2$ samples were heated at 840 °C and 846 °C, respectively, to grow the nuclei to observable-sized crystals.

Following the two-step heat treatments, the samples were polished with 400, 600, and 800 grit SiC papers and a 0.5 μm CeO_2 suspension (Allied High Tech Products Inc.). To rule out possible surface crystallization, at least 150 μm thickness of the surfaces of the samples were removed by polishing. The samples were then etched in a 0.2 HCl 0.5 HF (vol%) water solution for 10 s. After etching, the samples were washed in deionized water, then ultrasonically cleaned in acetone and deionized water separately, and dried on tissue paper in the air.

Microscopy images were obtained from different surface polished regions of the partially crystallized glass using an Olympus BX41M-LED optical microscope. A typical image for a $BaO{\cdot}2SiO_2$ heat-treated glass is shown in Fig. 1; the crystals have an irregular shape. For this case, the area of the crystal in the image was measured, treating the irregular shape as a sphere with a diameter corresponding to the measured area of the crystal. The correction equation for spherical crystals (Eq. (1)) was then used to calculate the number of crystals per unit volume, N_V

$$N_V = \frac{2}{\pi} N_S \overline{Y}, \tag{1}$$

where N_S is the number of crystals measured per area in the image and

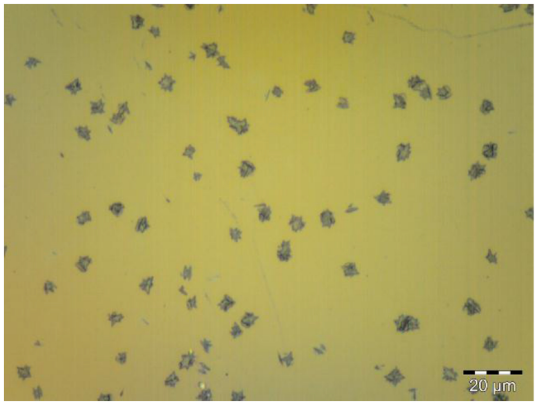

Fig. 1. Typical image observed in optical microscope for a $BaO{\cdot}2SiO_2$ glass that was heat treated at 725 °C for 9 min to develop a population of nuclei; these were grown to observable size by a second heat treatment at 840 °C.

$\overline{Y}$ is the average of the reciprocal diameters in the image [15,16]. Overlapping crystals were not used to determine the diameter, but were still counted to obtain the number of crystals per unit area. If the overlapping was so great that the number of crystals could not be counted, the image was not used for the analysis. Instead, a different growth treatment time was chosen to produce less crystal overlap. A typical image of the crystals in the $5BaO{\cdot}8SiO_2$ glass is shown in Fig. 2; unlike the crystals in $BaO{\cdot}2SiO_2$, these have spherical shapes. The diameters of each crystal in the image could then be measured directly and used to compute N_V. This was repeated for the data obtained for all of the nucleating temperatures. The standard deviation in N_V was calculated from the different images at each nucleation treatment.

Corrections to N_V were also made for the fraction underestimated due to the resolution limit of the microscope [17] and the nuclei density in the as-quenched glass. The resolution limit correction was made by assuming that crystal growth during the nucleation heat treatment was negligible so that the correction for a monodisperse system could be used [17]. For this, the fraction underestimated, f, is given by

$$f = \frac{2}{\pi} \sin^{-1}\left(\frac{\varepsilon}{d_M}\right) \tag{2}$$

ε is the microscope resolution limit and d_M is the maximum diameter observed in the sample. Here, ε is 0.45 μm for the 50× objective lens used. The nuclei density in the as-quenched glass was measured by heating the glass at the growth temperature without a prior nucleation treatment and using the image analysis method discussed above. The as-quenched nuclei data were also corrected for the microscope resolution.

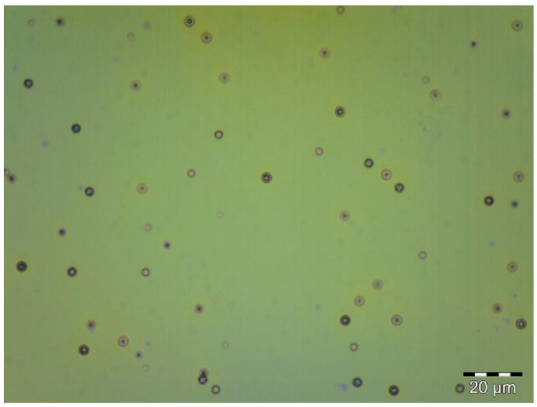

Fig. 2. Typical image observed in optical microscope for $5BaO{\cdot}8SiO_2$ glass that was heat treated at 700 °C for 57 min to develop a population of nuclei; these were grown to observable size by a second heat treatment at 846 °C.

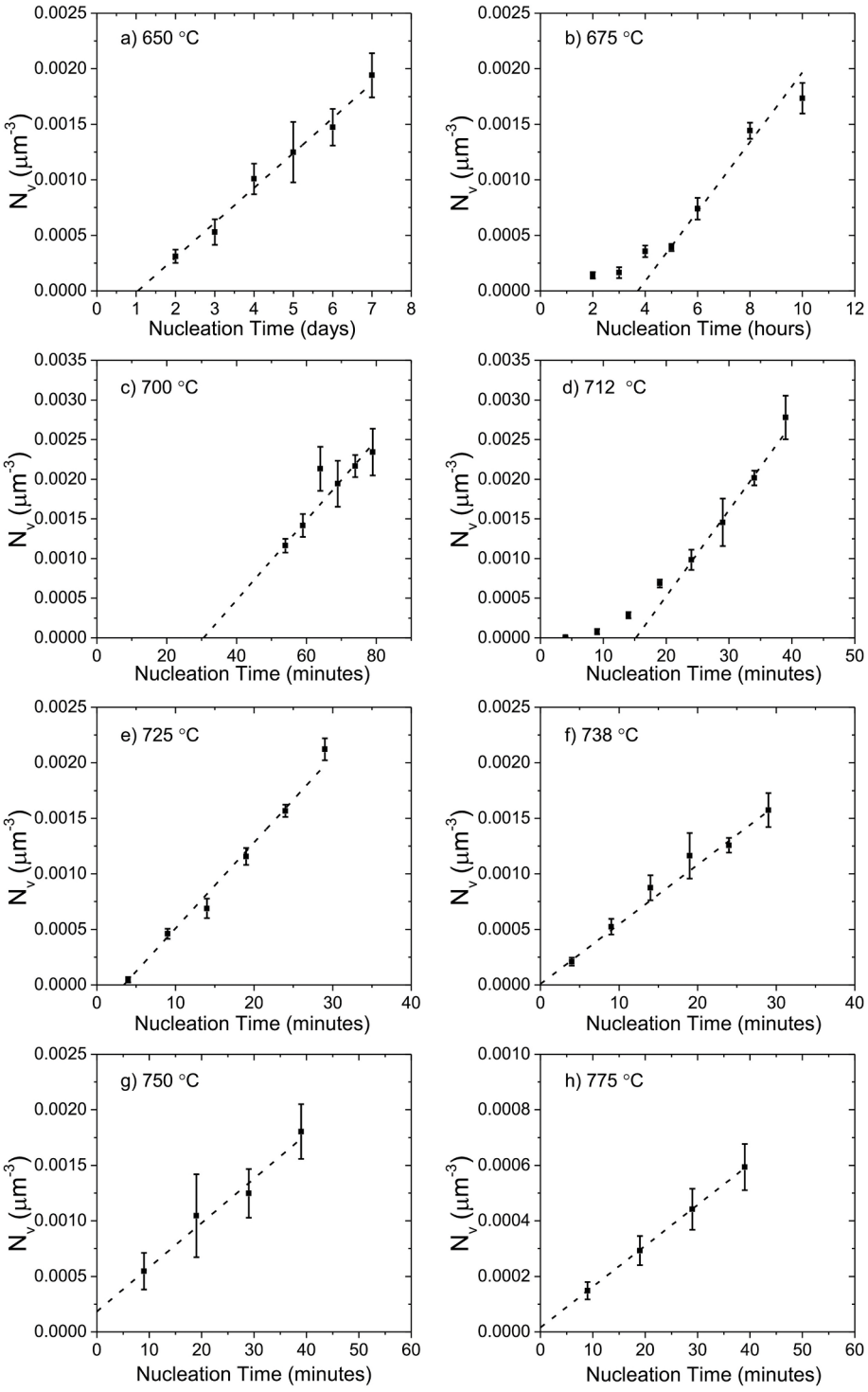

Fig. 3. N_V as a function of time at the nucleation temperatures studied for the $BaO{\cdot}2SiO_2$ glasses. The dashed lines show the linear fits in the steady-state used to determine I^{st}. (The error bars on the data are equal to the standard deviation in N_V calculated from the different microscope images at each temperature and heat treating time.)

3. Results

3.1. $BaO{\cdot}2SiO_2$

The values of N_V for the $BaO{\cdot}2SiO_2$ glass are shown as a function of the heat treatment time at the nucleating temperature in Fig. 3. Initially, N_V increases nonlinearly with time, reflecting a time-dependent nucleation rate. After some time it increases linearly with time, reflecting a steady-state nucleation rate; the steady-state nucleation rate, I^{st}, is given by the slope of N_V vs. time in this region. The intercept of the line with the time axis is the induction time at the critical size for the growth temperature, $\theta_{n*}^{T_G}$ [8]. The measured values for $I^{st}$and $\theta_{n*}^{T_G}$ are

Table 1
Steady state rates and induction times for nucleation in $BaO{\cdot}2SiO_2$ glasses.

Temperature, T (°C)[a]	Steady state nucleation rate, I^{st} ($mm^{-3}\,s^{-1}$)	Induction time, $\theta_{n*}^{T_G}$ (min)
650	3.6 ± 0.2	1501 ± 195
675	87 ± 9	222 ± 15
700	841 ± 98	31 ± 4
712	1812 ± 134	15 ± 1
725	1288 ± 46	3.4 ± 0.4
738	895 ± 41	Not determined
750	665 ± 61	Not determined
775	246 ± 2	Not determined

[a] The value and standard error were obtained from the linear fit in the N_V vs. nucleation time graphs using the instrumental weighting in Origin software.

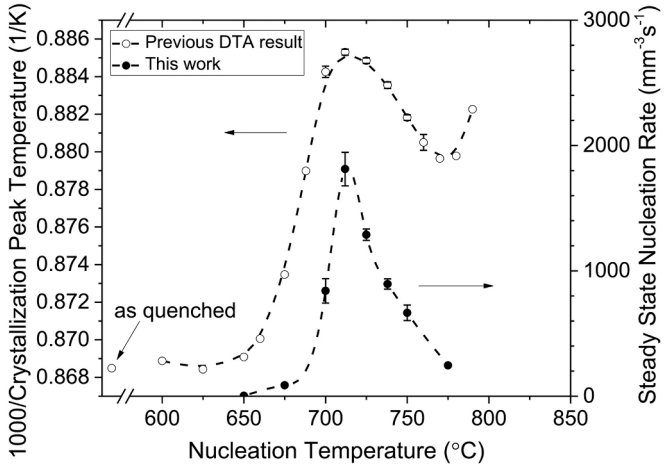

Fig. 4. The steady state nucleation rate and the inverse DTA crystallization peak temperature (which tracks with the nucleation rate – see [14]) versus the nucleation temperature for $BaO{\cdot}2SiO_2$ glasses.

listed in Table 1. The induction times are very short for the temperatures 738 °C, 750 °C and 775 °C and could not be obtained from the data; the negative intercepts are not physical but reflect the measurement uncertainty.

As shown in Fig. 4, the measured steady state nucleation rate has a maximum at 712 °C. This is in agreement with a previous estimate made from DTA studies [14]. The measured width of the nucleation rate (i.e. the temperature range for significant nucleation) is also in agreement with the DTA estimates. The range is approximately 675 °C to 775 °C for the directly measured nucleation rate data presented here. The range estimated in the DTA studies was from approximately 660 °C to 770 °C [14].

3.2. $5BaO{\cdot}8SiO_2$

The measured values of N_V for the $5BaO{\cdot}8SiO_2$ glass are shown as a function of the heat treatment time at the nucleating temperature in Fig. 5. As for the $BaO{\cdot}2SiO_2$ glass, the crystal nucleation rate is time-dependent, reaching the steady-state value after a sufficiently long heat treatment at the nucleation temperature. The values of I^{st} and $\theta_{n*}^{T_G}$, obtained from a linear fit to the steady-state region, are summarized in Table 2. The induction time at 775 °C could not be obtained since the intercept was negative, again reflecting the measurement error for short induction times.

The measured steady state nucleation rate has a maximum at 725 °C (Fig. 6). Like the $BaO{\cdot}2SiO_2$ glass, this result is in agreement with an estimation made from previous DTA studies [14]. The temperature ranges for significant nucleation in the data measured here are also similar to those estimated in the DTA studies.

4. Methods of analysis

4.1. Method #1

The measured data are analyzed using the CNT [8] for homogeneous nucleation of spherical clusters, with I^{st} (number per volume per second) given by

$$I^{st} = \frac{k_{n*}^{+} Z N_A}{V_m} \exp\left(-\frac{W^*}{k_B T}\right). \tag{3}$$

Here k_{n*}^{+} is the rate of single monomer attachment to the critical cluster of size n^*, Z is the Zeldovich factor, N_A is the Avogadro's number, V_m is the molar volume, W^* is the critical work of cluster formation, k_B is the Boltzmann constant and T is the temperature in absolute units. For spherical clusters, n^* is given by

$$n^* = \frac{32\pi}{3\bar{v}} \frac{\sigma^3}{|\Delta g_v|^3}, \tag{4}$$

where σ is the interfacial free energy, $\bar{v}$ is the volume of a monomer ($\bar{v} = V_m/N_A$), and Δg_v is the Gibbs free energy difference between the initial and nucleating phase per unit volume. For spherical clusters, the critical work of cluster formation, W^*, is

$$W^* = \frac{16\pi}{3} \frac{\sigma^3}{|\Delta g_v|^2}. \tag{5}$$

The Zeldovich factor in Eq. (3) is given by

$$Z = \left(\frac{|\Delta\mu|}{6\pi k_B T n^*}\right)^{1/2}, \tag{6}$$

where $\Delta\mu$ is the change in chemical potential for a monomer moving from the initial phase to the nucleating phase. $\Delta\mu$ is related to Δg_v as $\Delta\mu = \Delta g_v \bar{v}$. From the Kashchiev treatment [18,19], the induction time at the critical size for the nucleating temperature, θ, is related to the transient time, τ_K

$$\theta = \frac{\pi^2}{6}\tau_K, \tag{7}$$

which is a fundamental time describing the evolution of the cluster distribution and is given by

$$\tau_K = -\frac{24 k_B T n^*}{\pi^2 k_{n^*}^{+} \Delta\mu} = \frac{4}{\pi^3 k_{n^*}^{+} Z^2}. \tag{8}$$

Since the forward rate constant, $k_{n^*}^{+}$ can be extracted from the induction time, there is no need to assume a relation between $k_{n^*}^{+}$ and the diffusion coefficient or viscosity in the parent phase. The product of the steady state nucleation rate and the induction time, then, contains no kinetic terms,

$$I^{st}\theta = \frac{2}{3\pi\bar{v}Z} \exp\left(-\frac{W^*}{k_B T}\right). \tag{9}$$

Taking the natural logarithm of Eq. (9) and using the values for W^* in Eq. (5) and Z in Eq. (6),

$$\ln(I^{st}\theta) = \ln\left(\frac{16}{3\bar{v}^2}\right) + \frac{1}{2}\ln\left(\frac{\sigma^3 k_B T}{|\Delta g_v|^4}\right) - \left(\frac{16\pi}{3k_B}\frac{1}{T|\Delta g_v|^2}\right)\sigma^3. \tag{10}$$

The induction time measured in the two-step experiments is the value at the critical size for the growth temperature, T_G, i.e. $\theta_{n*}^{T_G}$. However, θ in Eq. (10) is the induction time at the critical size for the

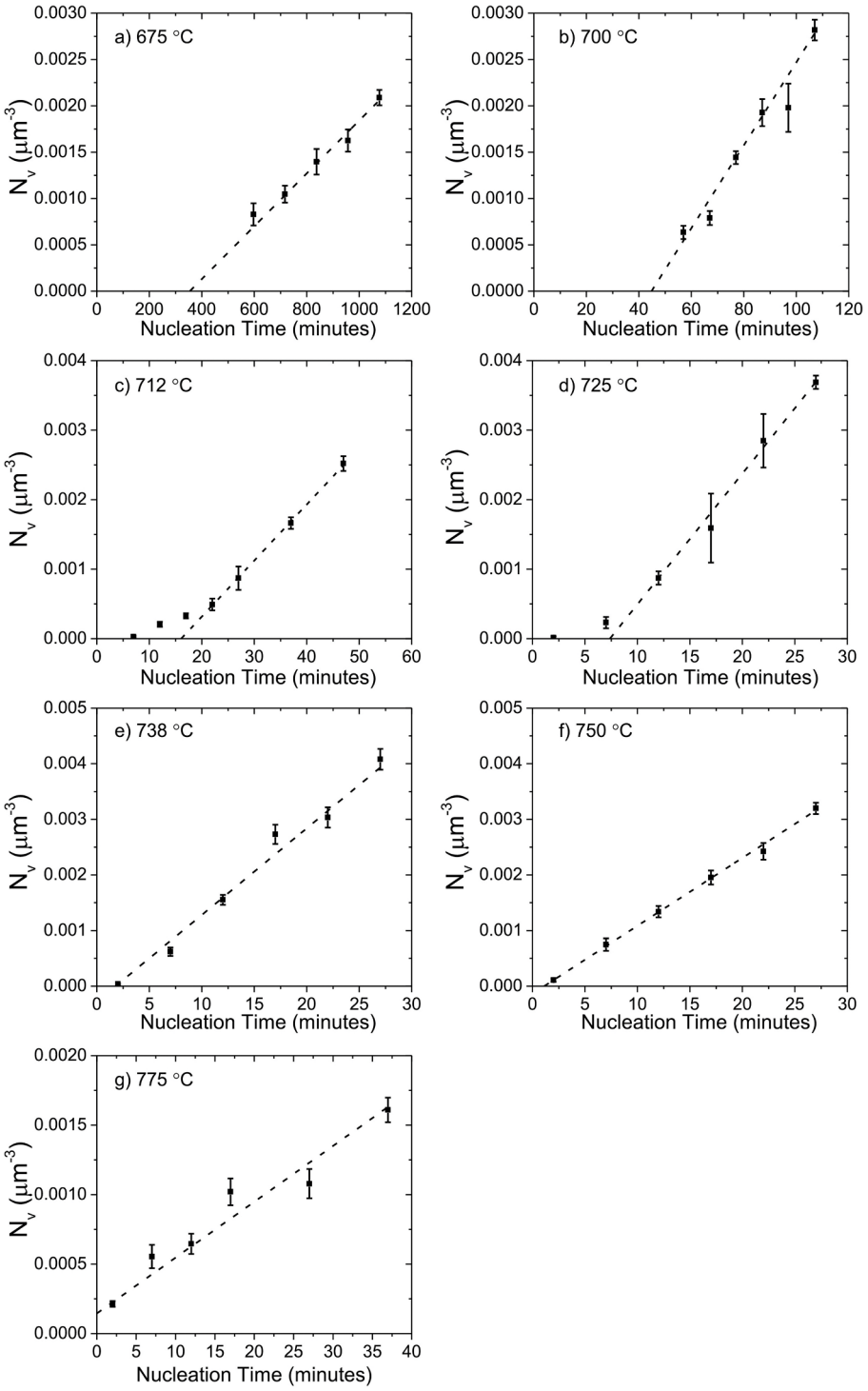

Fig. 5. N_V as a function of time at the nucleation temperatures studied for the $5BaO{\cdot}8SiO_2$ glasses. The dashed lines show the linear fits in the steady-state used to determine I^{st}. (The error bars on the data are equal to the standard deviation in N_V calculated from the different microscope images at each temperature and heat treating time.)

nucleation temperature, T_N, i.e. $\theta_{n*}^{T_N}$. The time required for a cluster to grow from n^* at T_N to n^* at T_G must therefore be taken into account. An equation that relates $\theta_{n*}^{T_N}$ to $\theta_{n*}^{T_G}$ is [8,20],

$$\frac{\theta_{n*}^{T_G}}{\theta_{n*}^{T_N}} = \frac{6}{\pi^2}\left[\xi + \ln\xi + \ln\left(\frac{6W^*}{k_B T}\right) + \zeta_E - 1\right], \tag{11}$$

where ζ_E is Euler's constant (0.5772…) and

$$\xi = \left(\frac{n_{T_G}^*}{n_{T_N}^*}\right)^{1/3} - 1 = \left(\frac{\sigma_{T_G}}{\sigma_{T_N}}\right)\Big/\left(\frac{|\Delta g_v|_{T_G}}{|\Delta g_v|_{T_N}}\right) - 1; \tag{12}$$

W^* is calculated from Eq. (5), using $\sigma_{T_N}$and $|g_v|_{T_N}$. By using Eq. (11) and Eq. (12), Eq. (10) can be modified to have the form

Table 2
Steady state rates and induction times for nucleation in $5BaO{\cdot}8SiO_2$ glasses.

Temperature, T (°C)[a]	Steady state nucleation rate, I^{st} ($mm^{-3}\,s^{-1}$)	Induction time, $\theta_{n*}^{T_G}$ (minutes)
675	48 ± 3	354 ± 41
700	746 ± 72	45 ± 4
712	1345 ± 25	16.1 ± 0.4
725	3135 ± 54	7.4 ± 0.3
738	2599 ± 127	1.8 ± 0.2
750	2035 ± 28	1.1 ± 0.1
775	669 ± 53	Not Determined

[a] The value and standard error were obtained from the linear fit in the N_V vs. nucleation time graphs using the instrumental weighting in Origin software.

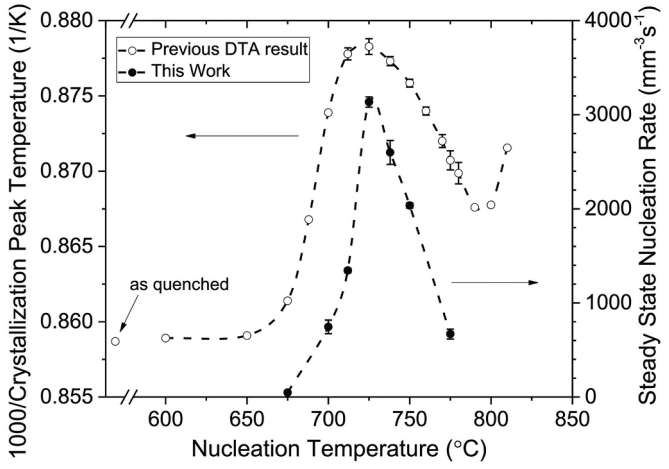

Fig. 6. Steady state nucleation rate and inverse DTA crystallization peak temperature [14] versus nucleation temperature for $5BaO{\cdot}8SiO_2$ glasses.

$$\ln\left(I^{st}\theta_{n*}^{T_G}\right) = \ln\left\{\left(\frac{\sigma_{T_G}}{\sigma_{T_N}}\right)\Big/\left(\frac{|\Delta g_v|_{T_G}}{|\Delta g_v|_{T_N}}\right) + \ln\left[\left(\frac{\sigma_{T_G}}{\sigma_{T_N}}\right)\Big/\left(\frac{|\Delta g_v|_{T_G}}{|\Delta g_v|_{T_N}}\right) - 1\right] + \ln\left[\frac{32\pi}{k_B}\right] + \ln\left[\frac{(\sigma_{T_N})^3}{T_N\left(|\Delta g_v|_{T_N}\right)^2}\right] + \zeta_E - 2\right\} + \ln\left[\frac{32}{\pi^2\bar{\nu}^2}\right] + \frac{1}{2}\ln\left(\frac{(\sigma_{T_N})^3 k_B T_N}{\left(|\Delta g_v|_{T_N}\right)^4}\right) - \left(\frac{16\pi}{3k_B}\frac{1}{T_N\left(|\Delta g_v|_{T_N}\right)^2}\right)(\sigma_{T_N})^3. \quad (13)$$

I^{st} and $\theta_{n*}^{T_G}$ were obtained from the data presented here, while $\bar{\nu}$ and Δg_v at T_N and T_G were obtained from the literature or from experimental measurements. One monomer is assumed to be one formula unit. The only two unknown parameters in Eq. (13) are, therefore, the interfacial free energies at the growth and nucleation temperatures, σ_{T_G} and σ_{T_N} respectively. An iterative method is followed to determine these: (a) assume an initial value for σ_{T_G}; (b) use the measured values of I^{st} and $\theta_{n*}^{T_G}$ at each nucleating temperature to calculate σ_{T_N} from Eq. (13); (c) for T_N's at the temperature of the maximum steady state nucleation rate and above, linearly extrapolate σ_{T_N} to the growth temperature to obtain a new value for σ_{T_G}; (d) if the difference between the initial value of σ_{T_G} and the new one is larger than 10^{-5} J/m^2, take the new value of σ_{T_G} and perform the calculation again until it converges; (e) using the converged value of σ_{T_G}, calculate σ_{T_N} from Eq. (13) for T_N with known I^{st} and $\theta_{n*}^{T_G}$; (f) linear extrapolate σ_{T_N} of temperatures at and above the temperature for the maximum nucleation rate to higher temperatures to get σ_{T_N} for T_N whose I^{st} is known but $\theta_{n*}^{T_G}$ is unknown; (g) calculate W^*/k_BT and $\theta_{n*}^{T_N}$ for different T_N with Eqs. (5) and (11).

Because the errors in the two parameters σ_{T_G} and σ_{T_N} are unknown, errors in σ_{T_G} and σ_{T_N} cannot be directly calculated using Eq. (13). To estimate the error in σ_{T_N}, σ_{T_G} is assumed to have no error, i.e. the errors in Eq. (13) are propagated into the error in σ_{T_N}. Using the 95% confidence intervals for I^{st} and $\theta_{n*}^{T_G}$ as the input errors, the error in σ_{T_N} is calculated from Eq. (13) by assuming that only the parameters I^{st}, $\theta_{n*}^{T_G}$ and σ_{T_N} have an error. Then, the error in σ_{T_N} is used as an input into Eqs. (5) and (11) to calculate the error in W^*/k_BT and $\theta_{n*}^{T_N}$.

4.2. Method #2

It is widely assumed that the interfacial free energy obtained from nucleation data linearly increases with increasing temperature [8]. This is argued to be a consequence of the diffuse interface between the nucleating cluster and the parent phase [21–24]. Using σ_{T_N} for T_N at the temperature of the maximum steady state nucleation rate and above obtained from method #1, a linear fit with temperature was therefore made to get new σ_{T_N} for T_N lower than the temperature of maximum steady state nucleation rate. These new values for σ_{T_N} were used to calculate new $|\Delta g_v|_{T_N}$ for these low temperatures from Eq. (13). This was particularly important for the low nucleating temperatures where the critical sizes are small and the values computed from the thermodynamic properties measured for large samples might not be appropriate to describe small clusters. Finally, W^*/k_BT and $\theta_{n*}^{T_N}$ for these low temperatures were calculated from Eqs. (5) and (11). The estimated errors in these calculations follows the process discussed in Section 4.1.

5. Analysis results and discussion

From Eq. (10), when σ is assumed as a constant, a graph of $\ln(I^{st}\theta_{n*}^{T_N})$ as a function of $\frac{1}{T_N(|\Delta g_v|_{T_N})^2}$ (where T_N is the nucleating temperature) should produce a straight line. Using Eq. (11) to obtain $\theta_{n*}^{T_N}$ from $\theta_{n*}^{T_G}$, this graph is shown in Fig. 7. For Fig. 7, the Δg_v used was from the Turnbull approximation, which is the same as later discussed in Sections 5.1.1 and 5.2.1; a constant value for σ was assumed (0.100 J/m^2) [18].

While a straight line serves as a guide to the eye at higher temperatures in both glasses, a marked departure near the peak nucleation temperature is observed. While this has been observed previously in $BaO{\cdot}2SiO_2$ and other silicate glasses [25,26], it is particularly strong in these measurements. The reasons for this behavior remain unclear. This is explored in more detail in the following sections.

5.1. $BaO{\cdot}2SiO_2$

5.1.1. Results from Method #1

For the analysis of the data for the $BaO{\cdot}2SiO_2$ glasses, one monomer was assumed as one formula unit of monoclinic $BaO{\cdot}2SiO_2$ and V_m was 73.34×10^{-6} m^3/mol [27]. The Turnbull approximation was used to calculate Δg_v with an enthalpy of fusion equal to 37.5 kJ/mol and a liquidus temperature of 1420 °C [28]; the temperature-dependent values for $|\Delta g_v|$ are shown in Fig. 8a. They increase with decreasing temperature, as expected. The initial value of σ_{T_G} was chosen to be 0.106 J/m^2; the converged value was 0.117 J/m^2. The values computed for σ_{T_N}, W^*/k_BT and $\theta_{n*}^{T_N}$ from Eqs. (13), (5), and (11) using the converged σ_{T_G} are shown as a function of the nucleation measurement temperature in Fig. 8. The solid points in Fig. 8.b are the values for σ_{T_N} obtained by this procedure. The unfilled squares are the values of σ that result from a linear extrapolation of the values at and above the peak nucleation temperature to higher temperatures. The unfilled points in

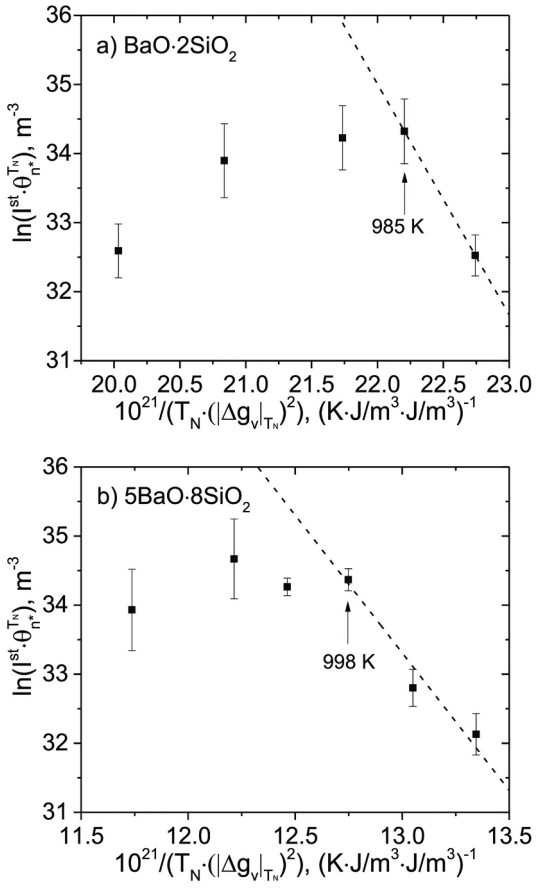

Fig. 7. $\ln(I^{st}\theta_{n*}^{T_N})$ as a function of $\frac{1}{T_N(|\Delta g_V|_{T_N})^2}$ in (a) $BaO{\cdot}2SiO_2$ and (b) $5BaO{\cdot}8SiO_2$ glasses with a straight line as a guide to the eye at high temperatures (the dashed lines). Errors were calculated using the 95% confidence intervals of I^{st} and $\theta_{n*}^{T_G}$.

Fig. 8.c for W^*/k_BT are calculated using the extrapolated points in Fig. 8b for σ. The curve of W^*/k_BT from the CNT was calculated assuming the Turnbull approximation for $|\Delta g_V|$ and a linear temperature dependence for σ_{T_N}.

Radically different results are observed for temperatures above or below the temperature for the maximum steady-state nucleation rate (985 K). As shown in Fig. 8b, the interfacial free energy increases above 985 K, as has commonly been found. However, it decreases with increasing temperature below 985 K. As shown in Fig. 8c, W^*/k_BT decreases with decreasing temperature at high temperatures, as expected within the CNT [26], but it plateaus and begins to slowly increase with decreasing temperature below 985 K. As normally observed, the log of the corrected induction time, $\theta_{n*}^{T_N}$, increases with increasing inverse temperature (Fig. 8d). From the Kashchiev expression Eq. (8), this reflects the increased mobility at higher temperatures.

5.1.2. Results from Method #2

Why the interfacial free energy would have such an abrupt change in temperature dependence below the peak nucleation rate temperature is difficult to understand. Based on other evidence, it should increase linearly with temperature [21–23]. To investigate this, the high temperature data in Fig. 8b were linearly extrapolated to lower temperature to force this agreement and to investigate further the deviation from CNT at lower temperatures (923 K, 948 K and 973 K). The result of the extrapolation is shown in Fig. 9a. Using these values for σ_{T_N}, $|\Delta g_v|_{T_N}$ was calculated from Eq. (13). As shown in Fig. 9b, this assumption of a linear temperature dependence causes $|\Delta g_V|$ to depart from the values expected from the Turnbull approximation and begin to decrease with decreasing temperature at 985 K. A similar behavior to that discussed in Fig. 8.c is again found for W^*/k_BT (Fig. 9c), with the value plateauing and then increasing with decreasing temperature, which is not the behavior expected from CNT, or even more advanced theories such as the diffuse interface theory or the semi-empirical density functional theory [21–23,29]. The temperature dependence of $\theta_{n*}^{T_N}$ remains essentially unchanged (Fig. 9d).

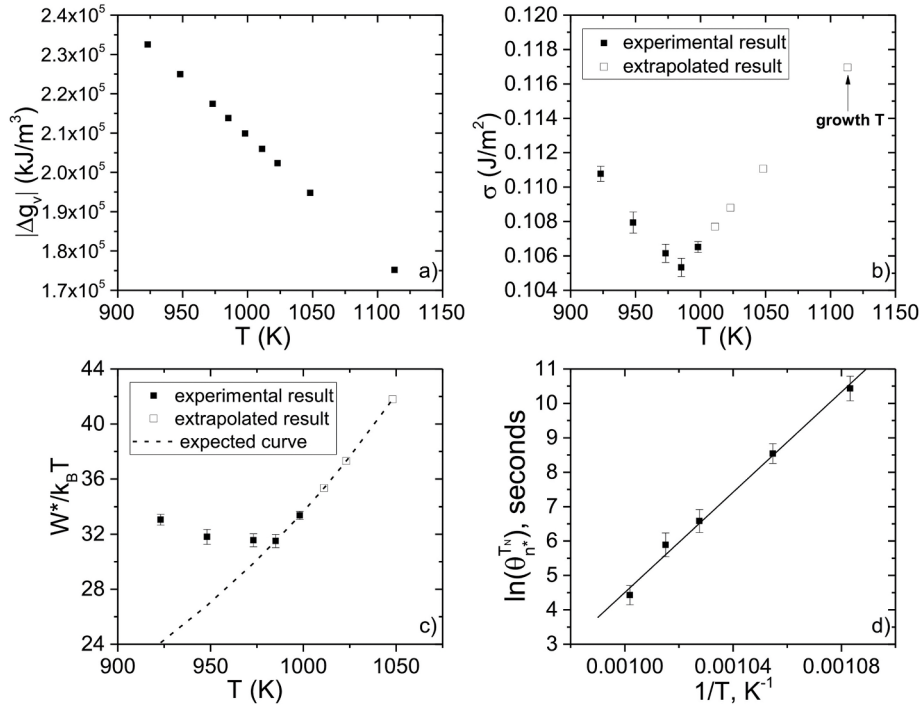

Fig. 8. The values of σ_{T_N}, W^*/k_BT and $\theta_{n*}^{T_N}$ from the measured nucleation data for the $BaO{\cdot}2SiO_2$ glasses: (a) $|\Delta g_V|$ as a function of temperature, (b) the calculated temperature dependence of the interfacial free energy, (c) the calculated values for W^*/k_BT as a function of temperature, (d) the log of the induction time as a function of inverse temperature. The errors were calculated using the 95% confidence intervals of I^{st} and $\theta_{n*}^{T_G}$.

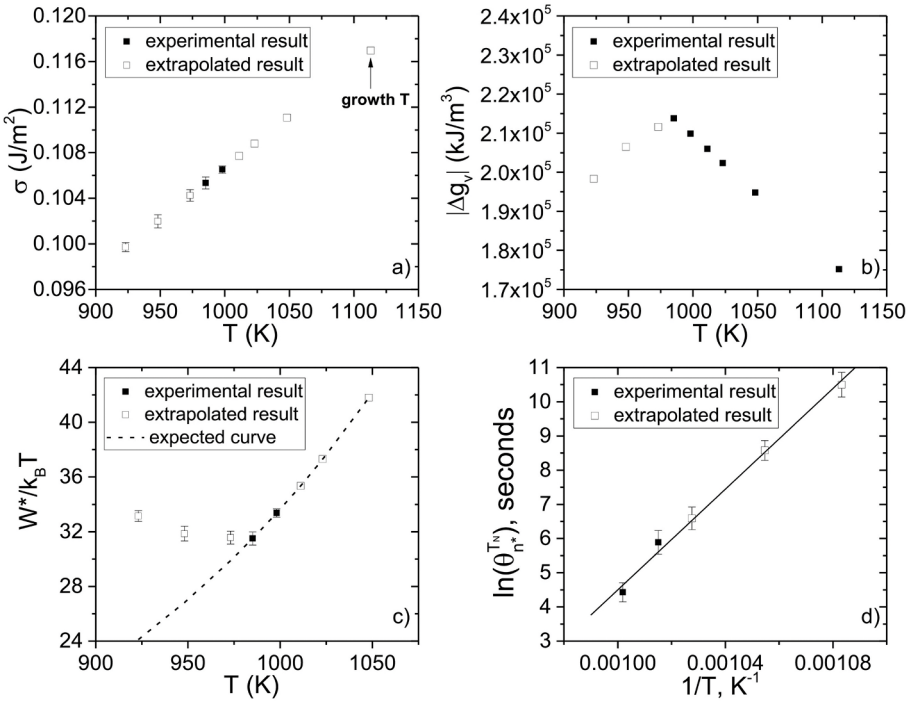

Fig. 9. The values of W^*/k_BT and $\theta_{n*}^{T_N}$ from the measured nucleation data for the $BaO{\cdot}2SiO_2$ glasses, assuming a linear temperature dependence of the interfacial free energy, σ_{T_N} (a): (b) the calculated values of $|\Delta g_V|$ as a function of temperature; (c) the calculated values for W^*/k_BT as a function of temperature; (d) the log of the induction time as a function of inverse temperature. The errors were calculated using the 95% confidence intervals of I^{st} and $\theta_{n*}^{T_G}$.

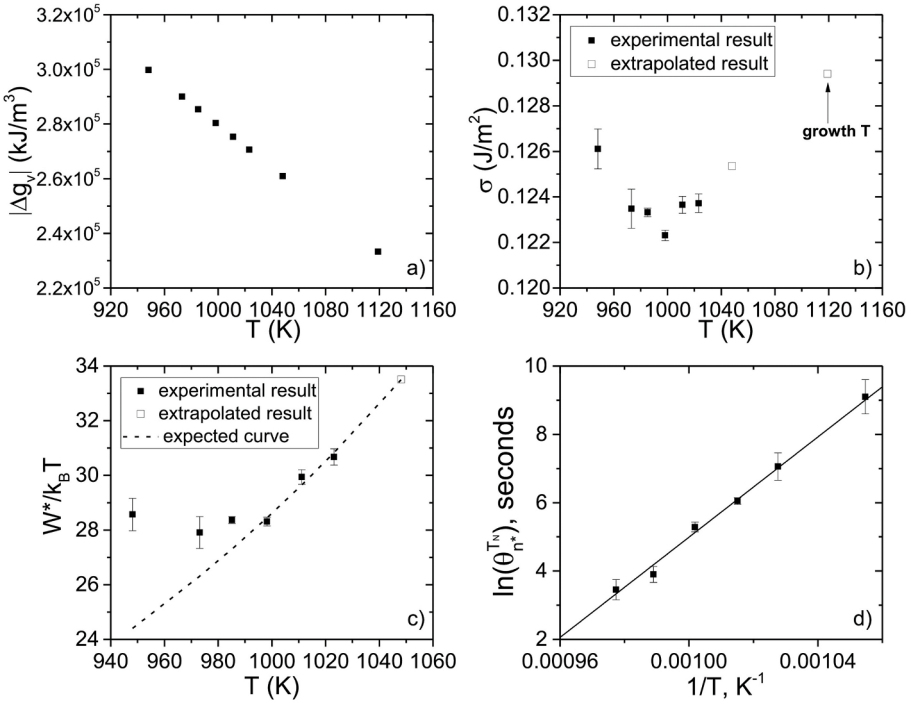

Fig. 10. The values of σ_{T_N}, W^*/k_BT and $\theta_{n*}^{T_N}$ from the measured nucleation data for the $5BaO{\cdot}8SiO_2$ glasses: (a) $|\Delta g_V|$ as a function of temperature, (b) the calculated temperature dependence of the interfacial free energy, (c) the calculated values for W^*/k_BT as a function of temperature, (d) the log of the induction time as a function of inverse temperature. The errors were calculated using the 95% confidence intervals of I^{st} and $\theta_{n*}^{T_G}$.

5.2. 5BaO·8SiO₂

5.2.1. Results from Method #1

The nucleation data in the $5BaO{\cdot}8SiO_2$ glass were analyzed following method similarly discussed in Section 4.1. One monomer was assumed as one formula unit of $5BaO{\cdot}8SiO_2$ and the value for V_m was taken as 317.7×10^{-6} m^3/mol, which was calculated from the monoclinic $5BaO{\cdot}8SiO_2$ structure (ICSD 100311). The value for Δg_v was calculated from the Turnbull approximation using the values of the enthalpy of fusion (212.3 kJ/mol) and the liquidus temperature (1446 °C), both obtained from DSC measurements. The values of Δg_v as a function of temperature are shown in Fig. 10.a. The initial value of σ_{T_G}

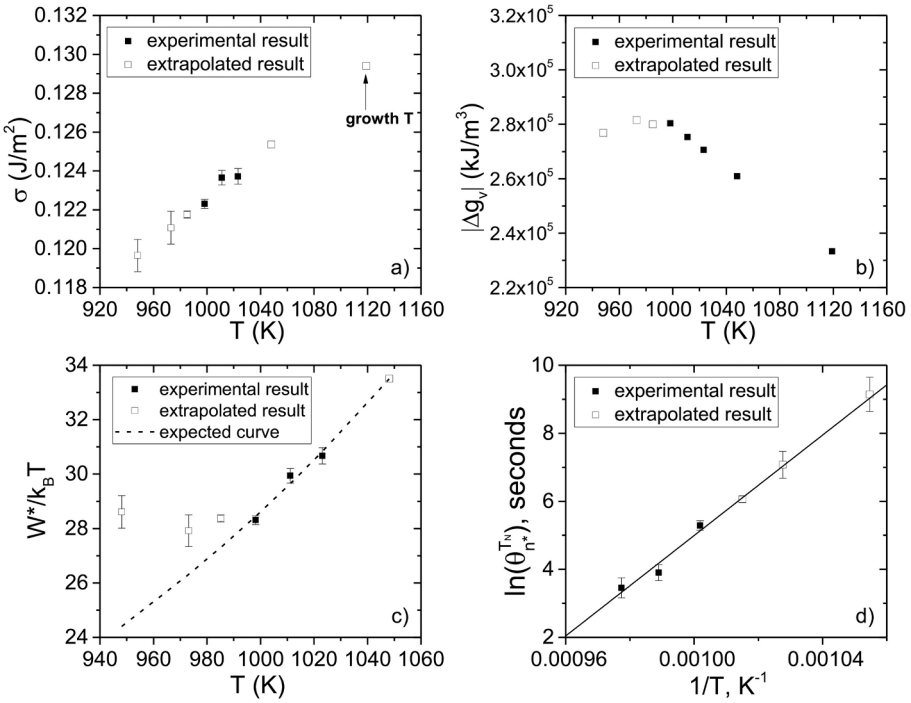

Fig. 11. The values of W^*/k_BT and $\theta_{n*}^{T_N}$ from the measured nucleation data for the $5BaO{\cdot}8SiO_2$ glasses, assuming a linear temperature dependence of the interfacial free energy, σ_{T_N} (a): (b) the calculated values of $|\Delta g_V|$ as a function of temperature; (c) the calculated values for W^*/k_BT as a function of temperature; (d) the log of the induction time as a function of inverse temperature. The errors were calculated using the 95% confidence intervals of I^{st} and $\theta_{n*}^{T_G}$.

was 0.113 J/m^2; it converged to 0.129 J/m^2. The calculated values for σ_{T_N}, W^*/k_BT and $\theta_{n*}^{T_N}$ using the converged value of σ_{T_G} are shown in Fig. 10b–d.

As for the $BaO{\cdot}2SiO_2$ glass, the calculated values of σ_{T_N} in the $5BaO{\cdot}8SiO_2$ glass change the sign of their temperature dependence near the peak nucleation temperature (998 K). Again, W^*/k_BT enters a plateau below this temperature (Fig. 10c), in disagreement with CNT and other more advanced nucleation theories. Also, as for $BaO{\cdot}2SiO_2$ glass, the logarithm of the induction time increases linearly with inverse temperature, reflecting the Arrhenius temperature dependence of the atomic mobility.

5.2.2. Results from Method #2

Again following the approach already discussed for the $BaO{\cdot}2SiO_2$ glass, the high temperature values of σ were linearly extrapolated to lower temperatures (Fig. 11a) and the values of $|\Delta g_v|_{T_N}$, W^*/k_BT and $\theta_{n*}^{T_N}$ were calculated using these values of σ. Again, this causes $|\Delta g_V|$ to decrease below the peak nucleation rate temperature (Fig. 11b). The values of W^*/k_BT still reach a plateau below that temperature (Fig. 11c), which is in conflict with all known theories of nucleation. The logarithm of the induction time still scales with inverse temperature (Fig. 11d).

A consistent picture emerges from these studies. In both glasses, there is a radical change of trend in the critical work of cluster formation (nucleation barrier) for temperatures below the peak in the nucleation rate. A similar behavior has been observed previously in other silicate glasses [26,30]. Some investigators have tested possible theoretical explanations such as elastic stress, changing size of structural units, spatial heterogeneity and dynamical heterogeneity to account for the effect [26,30–32], but the correct explanation remains unclear due to the lack of experimental or modeling evidence. While based on computer studies and more advanced models for nucleation a failure of CNT is expected at temperatures when the system is far from equilibrium, it is possible that at low temperatures, below that for the maximum steady state nucleation rate, the nucleation times used are inadequate to reach the steady-state. If CNT did not fail, however, the low temperature data would require a much longer nucleation treatment than any reported to date to our knowledge. For example, based on the discrepancy in Fig. 7, the 650 °C data point for $BaO{\cdot}2SiO_2$ would require approximately 1 year to reach the steady state nucleation rate.

6. Conclusions

In summary, the steady state nucleation rates and induction times were measured at multiple temperatures in $BaO{\cdot}2SiO_2$ and $5BaO{\cdot}8SiO_2$ glasses using the two-step heat treatment method. For $BaO{\cdot}2SiO_2$ glass, the steady-state nucleation rate has a maximum at 712 °C. For $5BaO{\cdot}8SiO_2$ glass, the maximum rate is at 725 °C. These results are in agreement with previous estimates made from differential thermal analysis measurements.

A new iterative method was introduced to calculate the interfacial free energy and critical work of cluster formation. For both glasses, the critical work of cluster formation shows an anomalous behavior, entering a plateau and slowly increasing rather than decreasing with decreasing temperature at low temperatures. This behavior either arises from an abrupt change in the temperature dependence of the interfacial free energy or decrease in the driving free energy for nucleation. The change in driving free energy is more likely, since the positive temperature dependence of the interfacial free energy arises from the diffuse interface between the cluster and the parent phase, which probably becomes even more diffuse at lower temperatures. The departure in the temperature dependence of the nucleation barrier is in disagreement with all known theories of nucleation. As we will explain in a future publication, using a Grand Canonical Monte Carlo simulation technique [33], we suggest that it arises from a closing-off of the nucleation pathways at lower temperatures. Finally, revisiting a point made at the end of the last section, to absolutely confirm that the critical work of cluster formation at low temperature is real, the time required for the nucleation step will need to be far longer than what was measured in this work and to our knowledge for any existing experimental reports to date.

Declaration of Competing Interest

The authors declare that they have no known competing financial interests or personal relationships that could have appeared to influence the work reported in this paper.

Acknowledgements

The authors thank L. Cai, A. Gangopadhyay, R. Ashcraft, R. Dai, M. Sellers, R. Chang for useful discussions. The figures were prepared using Origin software (Origin (Academic), Version 2016, OriginLab Corporation, Northampton, MA, USA). This work is financially supported by a NSF GOALI grant, DMR 17-20296, and by Corning Incorporated.

References

[1] J.C. Mauro, C.S. Philip, D.J. Vaughn, M.S. Pambianchi, Glass science in the United States: current status and future directions, Int. J. Appl. Glas. Sci. 5 (2014) 2–15.
[2] J.C. Mauro, E.D. Zanotto, Two centuries of glass research: historical trends, current status, and grand challenges for the future, Int. J. Appl. Glas. Sci. 5 (2014) 313–327.
[3] J.C. Mauro, Grand challenges in glass science, Front. Mater. 1 (2014) 20.
[4] W. Höland, V. Rheinberger, M. Schweiger, Control of nucleation in glass ceramics, Philos. Trans. Royal Soc. A 361 (2003) 575–589.
[5] W. Holand, G.H. Beall, Glass-Ceramic Technology, John Wiley & Sons, 2012.
[6] M.J. Davis, E.D. Zanotto, Glass-ceramics and realization of the unobtainable: property combinations that push the envelope, MRS Bull. 42 (2017) 195–199.
[7] G.H. Beall, Design and properties of glass-ceramics, Annu. Rev. Mater. Sci. 22 (1992) 91–119.
[8] K.F. Kelton, A.L. Greer, Nucleation in Condensed Matter-Applications in Materials and Biology, Elsevier, Amsterdam, 2010.
[9] P.F. James, Kinetics of crystal nucleation in lithium silicate-glasses, Phys. Chem. Glasses 15 (1974) 95–105.
[10] K.L. Narayan, K.F. Kelton, First measurements of time-dependent nucleation as a function of composition in $Na_2O{\cdot}2CaO{\cdot}3SiO_2$ glasses, J. Non-Cryst. Solids 220 (1997) 222–230.
[11] E.G. Rowlands, PhD Thesis, University of Sheffield, 1976.
[12] E.D. Zanotto, P.F. James, Experimental tests of the classical nucleation theory for glasses, J. Non-Cryst. Solids 74 (1985) 373–394.
[13] A.M. Rodrigues, PhD Thesis, Federal University of São Carlos, 2014.
[14] X. Xia, I. Dutta, J.C. Mauro, B.G. Aitken, K.F. Kelton, Temperature dependence of crystal nucleation in $BaO{\cdot}2SiO_2$ and $5BaO{\cdot}8SiO_2$ glasses using differential thermal analysis, J. Non-Cryst. Solids 459 (2017) 45–50.
[15] R.T. DeHoff, F.N. Rhines, Determination of number of particles per unit volume from measurements made on random plane sections: the general cylinder and the ellipsoid, Trans. AIME 221 (1961) 975–982.
[16] E.D. Zanotto, PhD Thesis, University of Sheffield, 1982.
[17] E.D. Zanotto, P.F. James, A theoretical and experimental assessment of systematic errors in nucleation experiments, J. Non-Cryst. Solids 124 (1990) 86–90.
[18] K.F. Kelton, Crystal Nucleation in Liquids and Glasses, Solid State Physics, vol. 45, Academic Press, New York, 1991.
[19] D. Kashchiev, Solution of the non-steady state problem in nucleation kinetics, Surf. Sci. 14 (1969) 209–220.
[20] V.A. Shneidman, M.C. Weinberg, Induction time in transient nucleation theory, J. Chem. Phys. 97 (1992) 3621–3628.
[21] F. Spaepen, Homogeneous Nucleation and the Temperature Dependence of the Crystal-Melt Interfacial Tension, Solid State Physics, vol. 47, Academic Press, Boston, 1994.
[22] L. Gránásy, Diffuse interface theory of nucleation, J. Non-Cryst. Solids 162 (1993) 301–303.
[23] L. Gránásy, Diffuse interface model of crystal nucleation, J. Non-Cryst. Solids 219 (1997) 49–56.
[24] D. Turnbull, Kinetics of solidification of supercooled liquid mercury droplets, J. Chem. Phys. 20 (1952) 411–424.
[25] M.C. Weinberg, E.D. Zanotto, Re-examination of the temperature dependence of the classical nucleation rate: homogeneous crystal nucleation in glass, J. Non-Cryst. Solids 108 (1989) 99–108.
[26] A.S. Abyzov, V.M. Fokin, A.M. Rodrigues, E.D. Zanotto, J.W. Schmelzer, The effect of elastic stresses on the thermodynamic barrier for crystal nucleation, J. Non-Cryst. Solids 432 (2016) 325–333.
[27] G. Oehlschlegel, Binary partial $BaO{\cdot}2SiO_2$-$2BaO{\cdot}3SiO_2$ system, Glastech. Ber. 44 (1971) 194–204.
[28] E.G. Rowlands, P.F. James, P.H. Gaskell (Ed.), The Structure of Non-Crystalline Solids, Taylor and Francis, London, 1977, p. 215.
[29] C.K. Bagdassarian, D.W. Oxtoby, Crystal nucleation and growth from the undercooled liquid: a nonclassical piecewise parabolic free-energy model, J. Chem. Phys. 100 (1994) 2139–2148.
[30] V.M. Fokin, A.S. Abyzov, E.D. Zanotto, D.R. Cassar, A.M. Rodrigues, J.W.P. Schmelzer, Crystal nucleation in glass-forming liquids: variation of the size of the “structural units” with temperature, J. Non-Cryst. Solids 447 (2016) 35–44.
[31] A.S. Abyzov, V.M. Fokin, N.S. Yuritsyn, A.M. Rodrigues, J.W.P. Schmelzer, The effect of heterogeneous structure of glass-forming liquids on crystal nucleation, J. Non-Cryst. Solids 462 (2017) 32–40.
[32] P.K. Gupta, D.R. Cassar, E.D. Zanotto, Role of dynamic heterogeneities in crystal nucleation kinetics in an oxide supercooled liquid, J. Chem. Phys. 145 (2016) 211920.
[33] M.E. McKenzie, J.C. Mauro, Hybrid Monte Carlo technique for modeling of crystal nucleation and application to lithium disilicate glass-ceramics, Comput. Mater. Sci. 149 (2018) 202–207.